

Bubble and spherical air shell formation dynamics

A. Tufaile* and J. C. Sartorelli

Instituto de Física, Universidade de São Paulo, Caixa Postal 66318, 05315-970 São Paulo, Brazil

(Received 6 May 2002; published 21 November 2002)

We studied the formation dynamics of air bubbles emitted from a nozzle submerged in aqueous glycerol solutions of different viscosities. We describe the evolution of the bubbling regimes by using the air flow rate as a control parameter and the time between successive bubbles as a dynamical variable. Some results concerning bubbling coalescence were emulated with a combination of simple maps. We also observed the formation of air shells surrounding liquid drops inside the liquid, known as antibubbles. The antibubbling conditions were related to an intermittent regime.

DOI: 10.1103/PhysRevE.66.056204

PACS number(s): 05.45.-a

I. INTRODUCTION

An antibubble is a striking kind of bubble in liquids that seemingly does not comply with buoyancy, and after few minutes disappears suddenly inside the liquid [1]. Unlike a simple air bubble that rises directly to the liquid surface, an antibubble wanders around in the fluid due to its slightly lower density than the surrounding liquid. In spite of this odd behavior, an antibubble can be understood as the opposite of a conventional soap bubble in air, which is a shell of liquid surrounding air; an antibubble is a shell of air surrounding a drop of liquid inside the liquid.

One of the most interesting aspects of this metastable object is its formation because this process involves simultaneously dripping and bubbling. This work is a sequel to our study of dynamical systems in bubble formation [2].

We found some conditions that produce antibubbles. For certain bubbling regimes, a large bubble is formed by coalescence between two consecutive smaller ones, followed by an inverted dripping of the fluid inside the air bubble due to an infolding process as shown in Fig. 1. By recording with a VHS camera, we followed the formation of some antibubbles as well as their trajectories driven by the liquid circulation.

Using the air flow rate as a control parameter, we characterized the dynamics by measuring the time between bubbles. We observed period doubling, intermittent behavior, abrupt enlargement of the attractor size due to the coalescence between bubbles [3], and antibubble formation.

II. EXPERIMENTAL APPARATUS

The experimental apparatus consists of a cylindrical tube with a diameter of 11 cm and 70 cm length with a column of an aqueous solution of glycerol, as shown in Fig. 2. This kind of solution was used due to its viscosity and transparency. The air is supplied at a constant flow through a solenoid valve controlled by a proportional, integral, and derivative (PID) controller connected to a large capacitive air reservoir. The bubbles are formed in a nozzle that is a tube with 0.78 mm inner diameter and 38 mm long placed at the bottom of the tube. The dynamics of bubble formation was studied with a noninvasive technique in the same way as was

done in the dripping faucet experiment (see Refs. [3,4] for details). A horizontal laser beam, placed 2 mm above the nozzle, is focused on a photodiode, so that we can detect the beginning or ending of scattering of the laser beam; delay times between successive bubbles were measured with homemade time circuitry in a PC computer. With the series of time intervals between bubbles $\{T\}$, we characterized the dynamics. Diagram bifurcations were constructed by letting the air flow rate decrease naturally to reduce bubbling (turning off the PID controller); the attractors were reconstructed with first return maps T_{N+1} vs T_N obtained keeping the air flow fixed; and the bubbling rate was calculated as $f_b = 1/\langle T \rangle$. All the measurements were done at room temperature. We also recorded the bubble formation with a VHS camera to illustrate their profiles corresponding to different dynamical behaviors and to observe the antibubble population. The bubbling is represented in Fig. 2 with two antibubbles captured in the liquid circulation.

The physical properties of the liquid phase were varied in the investigation by using the following solutions [% glycerol/% water (viscosity)] [5]: 0/100 (0.9 cP), 20/80 (1.6 cP), 34/66 (2.6 cP), 50/50 (5.1 cP), 60/40 (9.0 cP), 66/34 (14.5 cP), and 80/20 (47.0 cP). As the antibubbling regime is a particular state obtained from the bubbling system, we will first describe the route to reach this regime.

III. BUBBLING REGIMES

In Fig. 3 are shown, for six different solution concentrations, the respective bifurcation diagrams, on letting the air

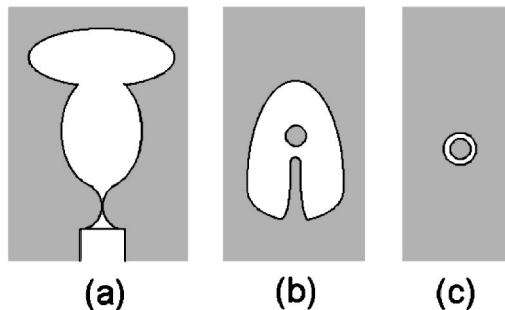


FIG. 1. Diagrams of (a) coalescence between two consecutive bubbles in (b) the inverted dripping inside the bubble after the coalescence, and (c) a cross section of an antibubble showing the internal drop.

*Corresponding author. Electronic address: tufaile@if.usp.br

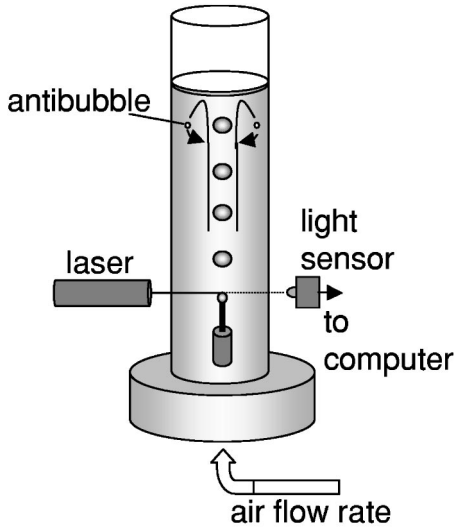


FIG. 2. The experimental apparatus with the bubbling rising in line and antibubbles captured in the liquid circulation.

flow decrease naturally along with the bubbling. As we can see the bifurcation from period 1 to period 2 becomes well defined when the solution viscosity is higher than 9.0 cP (60/40). Figure 4 is an illustration of the bubble profiles in both periodic regimes.

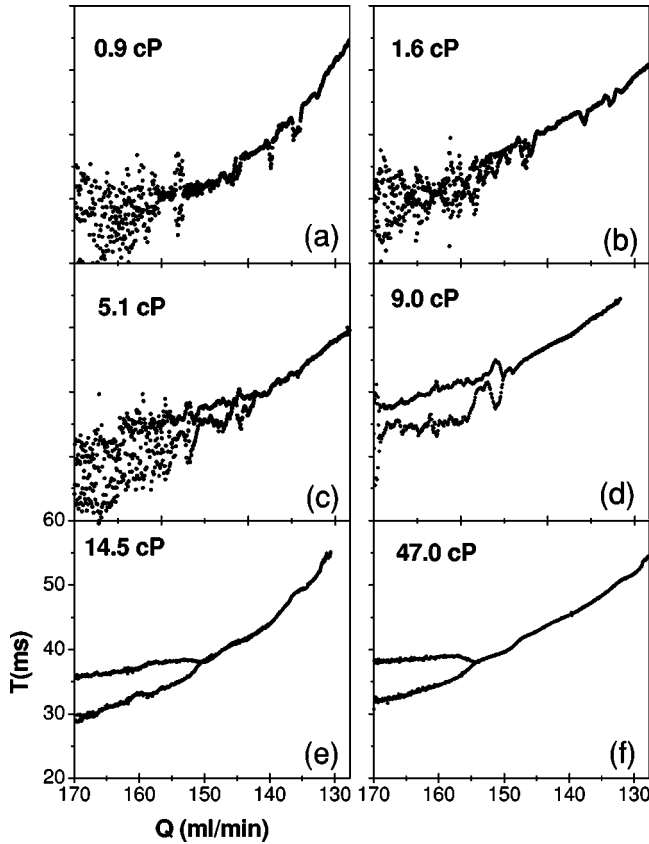


FIG. 3. Bifurcation diagrams obtained by letting the flow rate decrease naturally with bubbling for six different concentration solutions. From (a) to (f) the viscosity is increased by adding glycerol, as indicated in each frame. The liquid column is 5 cm high.

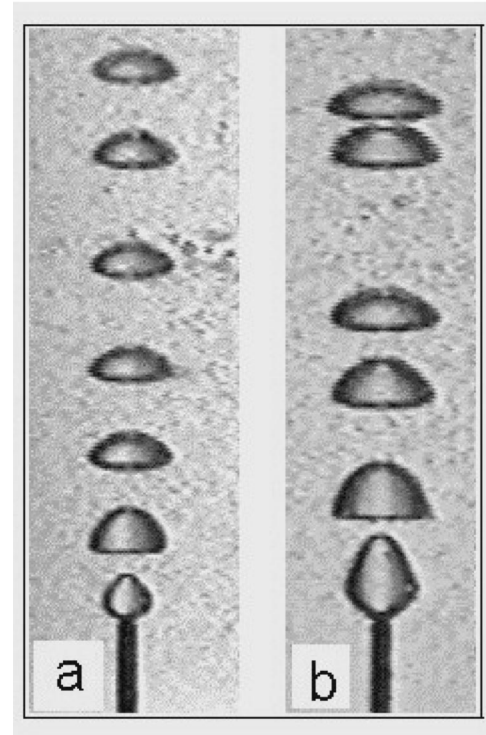


FIG. 4. Bubbling illustration of the case shown in Fig. 3(f). In (a) period-1 behavior ($Q = 135$ ml/min), (b) period-2 behavior ($Q = 165$ ml/min). The liquid solution is 80/20 (47 cP), and the liquid column is 15 cm high.

A. Periodic behavior

The time between bubbles in the period-1 behavior has a hyperbolic dependence on the air flow rate. It can be obtained following the simple assumptions for bubble formation at constant flow rates given by Davidson and Schüler [6], where the distance d between the center of the growing bubble and the nozzle is given by

$$d = \frac{2g}{15\nu} \left(\frac{3Q}{4\pi} \right)^{2/3} t^{5/3}, \quad (1)$$

where g is the gravity constant, ν is the kinematic viscosity of the liquid, Q is the flow rate, and t is the growing time of the bubble. For bubbling in period 1, a bubble is launched whenever the bubble radius exceeds the threshold R . In view of these assumptions, the time of bubble formation T is given by the equation

$$T = \left(\frac{15\nu R}{2g} \right)^{3/5} \left(\frac{4\pi}{Q} \right)^{2/5}, \quad (2)$$

which gives a hyperbolic relationship between the bubbling time and the air flow rate $F_b = (1/T) \sim Q^\beta$. The experimental values of the exponent β for three liquid viscosities and different column heights are shown in Table I. We observed that, in addition to the viscosity, the column height influences the bubbling dynamics, so the model is adequate for viscous liquids and for low column height. Nevertheless, the mean

TABLE I. The β values obtained experimentally at room temperature, as a function of the liquid column height (h) for three different viscosities (μ).

h (cm)	μ (cP)		
	47	15	0.9
5	0.40	0.42	1.26
12	0.43	0.47	0.80
26	0.56	0.58	0.79

time between bubbles still presents a hyperbolic dependence on the air flow rate with $\beta > 0.4$ for lower viscosity liquids and higher column heights.

Depending on the viscosity of the solution, the period-1 behavior can bifurcate to period 2, for more viscous fluids, or to random bubble emission for less viscous fluids. Considering these bifurcations as instabilities, we measured two dimensionless groups [7] related to the surface tension, viscous forces, and inertia at each period doubling, given by the Reynolds number (Re) and Eötvös number (Eo), also known as the Bond number,

$$Re = \frac{u d_e \rho}{\mu}, \quad (3)$$

$$Eo = \frac{g d_e^2 \rho}{\sigma}, \quad (4)$$

where ρ and μ are, respectively, the liquid density and the viscosity, u is the bubble speed, and σ is the surface tension. $d_e = (6V_b/\pi)^{1/3}$ is the diameter of an equivalent spherical bubble with volume V_b . A plot of Eo vs Re obtained with the experimental values of ρ , μ , u , and d_e is shown in Fig. 5. The $Eo \sim 2.7$ value is approximately independent of the Reynolds number, for different nozzles and viscosities, in the range from 200 up to 1500. The main source of the error in these measurements came from the diameter d_e .

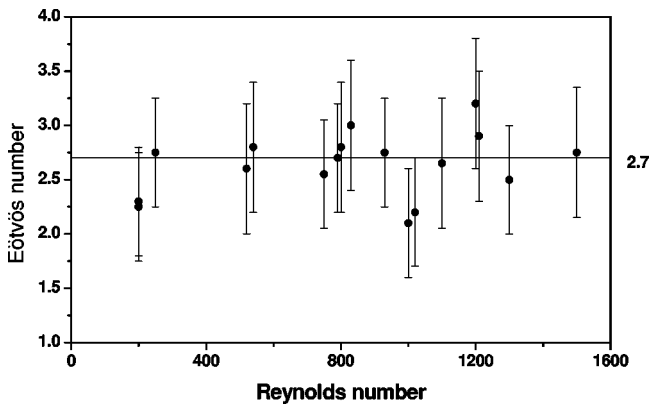


FIG. 5. For different values of Reynolds number the period doubling occurred at Eötvös number around 2.7.

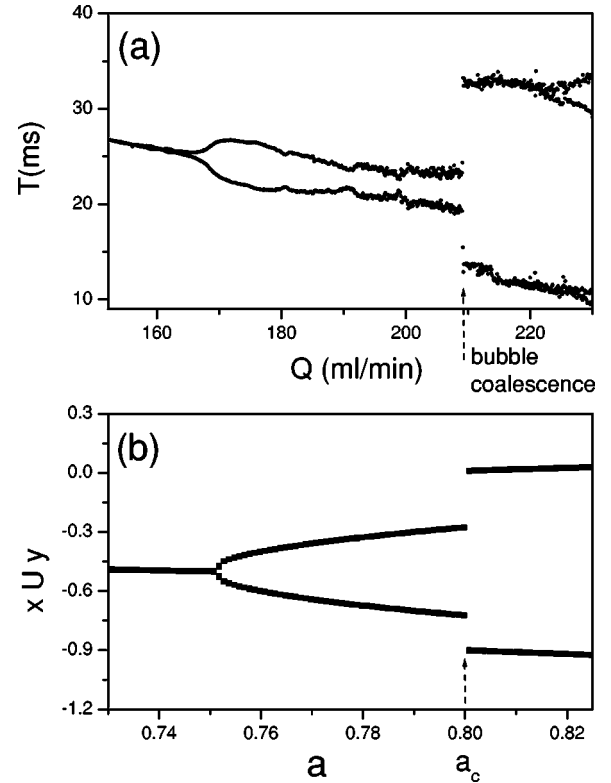


FIG. 6. Period doubling and coalescence in (a). This behavior was emulated with combined maps in (b). The liquid solution is 80/20 (47 cP), and the liquid column is 15 cm high.

B. The coalescence and combined maps

Figure 6(a) shows the experimental bifurcation diagram with the air flow rate as a control parameter. At a critical value of the flow rate ($Q_c \sim 210$ ml/min) a sudden change in the size of the period-2 attractor is observed, related to an increase of bubble size due to the coalescence process.

The mechanism of coalescence gives rise to singularities at the bubble interface, and an abrupt change in the time intervals is a signature of contact between bubbles, sustaining the idea that the dynamics has changed to another bubbling mode. Inspired by the behavior of the experimental time series, we considered a combination of quadratic maps in order to emulate such behavior in a simple way [4], as shown in Fig. 6(b). Expressing this contact between bubbles in terms of simple maps provides hints about the bubble growing mechanism, like the type of interaction between successive bubbles in terms of dynamical systems. We can emulate the first period doubling with a quadratic map given by

$$x_{n+1} = x_n^2 - a, \quad (5)$$

until the control parameter reaches the critical point a_c , where the two stable fixed points are replaced by two new ones. The enlargement in the size of the period-2 attractor observed experimentally can be interpreted by the combination of two interacting quadratic maps, for $a > a_c$, in which there is feedback of one quadratic map into the other one [see Fig. 6(b)]:

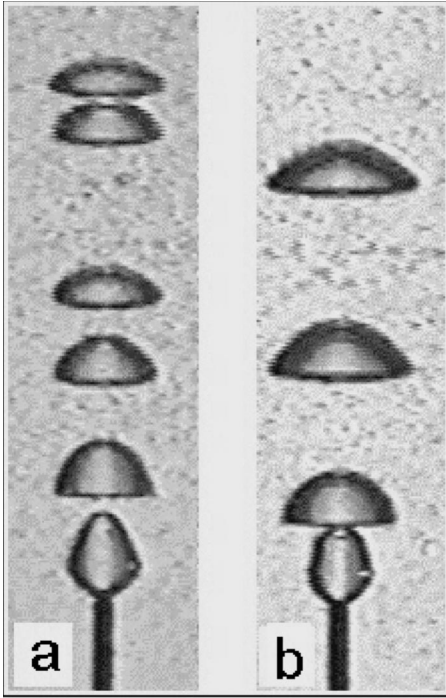


FIG. 7. (a) Bubble profile for a flow rate below $Q_c = 210$ ml/min without coalescence, and (b) the profiles, above Q_c , with bigger bubbles due to the effect of coalescence. The liquid conditions are the same as in Fig. 6.

$$\begin{aligned} x_{n+1} &= y_n^2 - a, \\ y_{n+1} &= x_n^2 - (a + 0.1). \end{aligned} \quad (6)$$

The coalescence between bubbles corresponds to the combination of maps in Eq. (6). The first bubble has a growth function the same as in the bubbling regime before time enlargement, which corresponds to the parameter a for the one-dimensional map emulation. After the detachment of this bubble, the second one starts to form in the same way as before; however, it is elongated in the vertical direction caused by the wake flow of the first bubble, and near the nozzle the two bubbles coalesce, forming a single large irregular bubble. This new bubble configuration is associated with a different control parameter ($a + 0.1$). The bubble profiles for flow rates below and above Q_c are shown in Fig. 7. An interesting feature of the combined maps of Eq. (6) is that the maximal dimension of the attractor obtained from each map is independent of the number of combined one-dimensional maps. This property enables us to reduce this system to two uncoupled iterations of second order for each branch of the bifurcation diagram:

$$\begin{aligned} x_{n+2} &= x_n^4 - 2(a + 0.1)x_n^2 + (a + 0.1)^2 - a, \\ y_{n+2} &= y_n^4 - 2ay_n^2 + a^2 + 0.1 - a. \end{aligned} \quad (7)$$

In Fig. 8 are shown the plots of these two functions and the respective fixed points x^* and y^* . Therefore, the sudden change in the bubble shape is analogous to a double-valued mapping. For higher flow rates, mutual interactions between

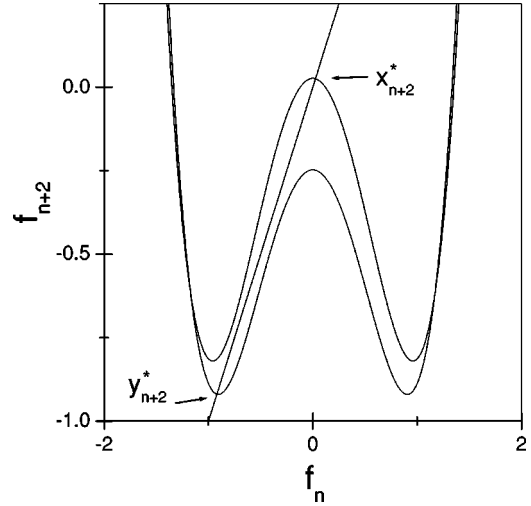


FIG. 8. The uncoupled functions representing the two different bubble growing stages. The fixed point $y(x^*)$ is associated with the bubble growth function for the first bubble and $x(y^*)$ represents the bubble growing after coalescence.

spatially separated bubbles can cause other sources of instabilities and give rise to spatiotemporal chaos [8,9].

IV. ANTIBUBBLES

Antibubble formation is a combination of bubbling and dripping processes. The coalescence described before is the genesis of the antibubbling regime, causing the existence of inverted dripping, as a consequence of the necking process by which the second bubble detaches from the nozzle. We present the mechanism of drop formation inside bubbles. After this, we obtained data for bubble formation during the antibubbling regime. The analysis of this time series indicates an intermittent transition to chaos, and the antibubbles are a consequence of this scenario.

A. Rayleigh jet and drop ejection

When two bubbles coalesce, the lower part of the bubble attached to the nozzle is pinched off and its neck contracts abruptly, causing a radial inrush of liquid as shown in Fig. 9(a). The fluid is rapidly accelerated inward and forms a Rayleigh jet [10,11] penetrating the coalesced bubble in an infolding process. In Fig. 9(b) this Rayleigh jet becomes unstable and breaks off one droplet. This droplet is not absorbed by the liquid, and travels to the surface inside the bubble [Fig. 9(c)]. This inverted dripping starts for a bubbling frequency around 50 bubble/s, and consequently the droplet formation is approximately one-half of this value, 25 drop/s.

The physical parameters that determine the inner drop formation are the inertial, viscous, and capillary forces that act as the two bubbles coalesce and begin the inverted dripping [12], and geometric parameters such as the needle size, bubble size, and liquid column height. Even though many of these drops are expelled from the liquid, some of them encounter the inner surface of the bubble, and a layer of air is trapped around the drop, preventing the drop ejection.

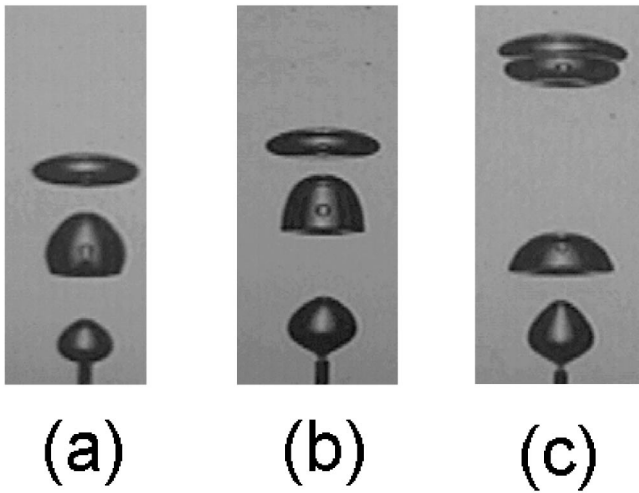


FIG. 9. The mechanism of antibubble formation is related to a small drop that occurs whenever a spike of liquid rushes into a bubble (a), until the interface is broken up (b), and a small fluid drop is formed inside the bubble (c). Some of these drops will be surrounded by air and captured by the liquid circulation. The liquid concentration is 66/34 (14.5 cP), and the flow rate is 230 ml/min, with bubbling of period 4.

B. Antibubbling regime and intermittency

At this point we are observing antibubble formation. In Fig. 10 we can see some antibubbles surrounding an intermittent bubbling regime. Although we have observed antibubble formation for different aqueous solutions and for different bubbling regimes, the antibubble stability depends on the liquid and bubbling regime. Some antibubbles are captured by the liquid moving around and break into tiny bubbles within 1 min; nevertheless, we commonly observed some of them to last up to 1 h. Just as a soap bubble pops because of gravity, due to the fact that the liquid accumulates at the bottom of the soap bubble, the lifetime of an anti-

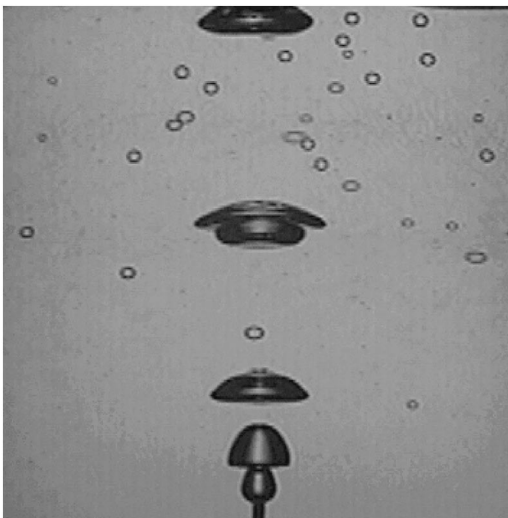


FIG. 10. Antibubbles surrounding the bubbling. The liquid solution is 66/34 (14.5 cP) for a flow rate of 265 ml/min. The liquid column is 15 cm high.

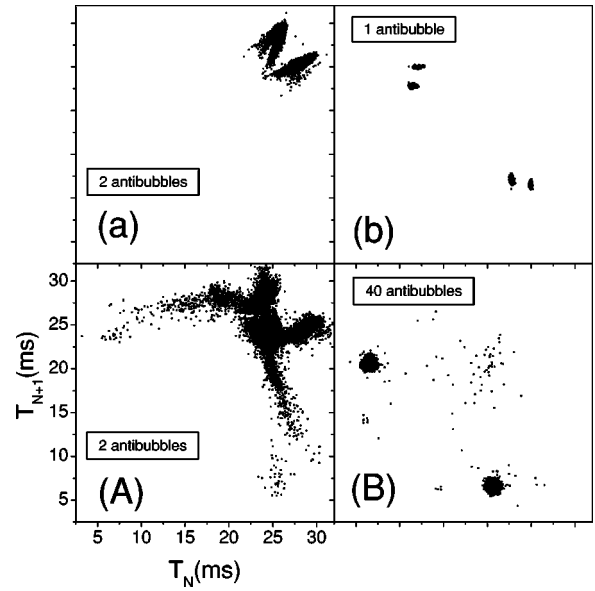


FIG. 11. For a liquid concentration 34/66 (2.6 cP) in (a) there is noisy period-4 behavior for air flow rate of 170 ml/min, and in (A) chaotic bubbling for the flow rate of 190 ml/min. In both cases we observed two antibubbles. For a solution with 66/34 (14.5 cP) for a flow rate of 235 ml/min the average number of antibubbles is 1 (b), and in (B) for the flow rate of 265 ml/min we obtained around 40 antibubbles.

bubble depends on the shape of the air shell, which becomes thinnest at the bottom and thickest at the top in time. The reason for some antibubbles to be more persistent than those of a static bath may be based on the assumption that the liquid circulation caused by the bubble formation causes the spherical shell of air to have uniform thickness. Despite the fact that an increase in the flow rate causes an increase in the size of bubbles, and consequently an increase in the size of the liquid spike inside the bubble, the maximal antibubble radius remained at 5 mm.

In Fig. 11 are shown some attractors from the bubbling obtained during antibubble formation with two different solutions. For a liquid 34/66 (2.6 cP) we observed bubbling with a noisy period-4 behavior for air flow rate of 170 ml/min in Fig. 11(a), and a chaotic bubbling for the flow rate of 190 ml/min in Fig. 11(A), with two antibubbles in both cases. For a solution with 66/34 (14.5 cP) for a flow rate of 235 ml/min the antibubble number is 1 for the attractor showing period 4 in Fig. 11(b). Increasing the flow rate still more, the period-4 attractor evolves to period 2 with intermittent bursts, represented by the spread points in Fig. 11(B) for the flow rate of 265 ml/min; and in this bubbling regime we obtained around 40 antibubbles. The second aqueous solution of glycerol (14.5 cP) presented the best results in antibubble production, so we concentrated our attention on this liquid. For the pure water case we did not find the antibubbling regime, even though we observed inverted dripping inside the air bubble.

To describe the route via intermittency we followed the same procedure adopted by Ruzicka *et al.* [13,14] to characterize the bubbling-to-jetting regime, so we calculated the distribution $D(L)$ of the number of bubbles L between two

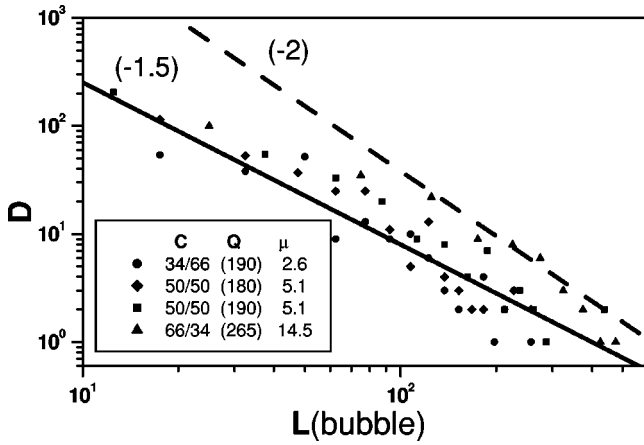


FIG. 12. The distribution $D(L)$ of the number of bubbles L between two bursts of chaos in a periodic motion for three different concentrations [or viscosities μ (cP)] with three different air flow rates Q (ml/min). Also drawn are the curves $D(L) \sim L^{-2}$ (dashed line) and $L^{-1.5}$ (continuous line). The comparison between these curves and the experimental data suggests that the intermittency is type III.

bursts of chaos in periodic motion. In Fig. 12 are shown the experimental data $D(L)$ obtained for three different viscosities with different air flow rates. A U-shaped distribution is typical for type I intermittency, while types II and III display a hyperbolic distribution $L^{-\gamma}$ with exponents equal to $\gamma = 2$ and $\gamma = 1.5$, respectively. By fitting $D(L) = AL^{-\gamma}$ to our four sets of experimental data, shown in Fig. 12, we obtained the γ values shown in Table II.

For comparison between the hyperbolic distributions and the experimental ones, we have also drawn $D(L) \sim L^{-2}$ (dashed line) and $D(L) \sim L^{-1.5}$ (continuous line) in Fig. 12. Therefore, the data are consistent with type III intermittency.

The balance between antibubble creation and annihilation gives an average population of antibubbles, the antibubble number. The antibubble number increases in the presence of intermittency, as is shown in Fig. 13, with a maximum value of 40 antibubbles for a flow rate of 265 ml/min. On increasing the air flow still more to 275 ml/min, the antibubble number decreased, due to strong uneven movements within liquid. The drop in the bubble frequency indicates bubble coalescence occurring very close to the nozzle, reinforcing the inverted dripping. For this liquid the chaotic regime seems to stimulate antibubble formation.

This is an experiment in which a temporal chaotic process generates spatial patterns and metastable structures. The bubble formation localized spatially on the nozzle creates a

TABLE II. γ values obtained by fitting $D(L)$ to the experimental data shown in Fig. 12.

C	μ (cP)	Q (ml/min)	$\gamma \pm 0.2$
34/66	2.6	190	1.5
50/50	5.1	180	1.5
50/50	5.1	180	1.7
66/34	14.5	265	1.6

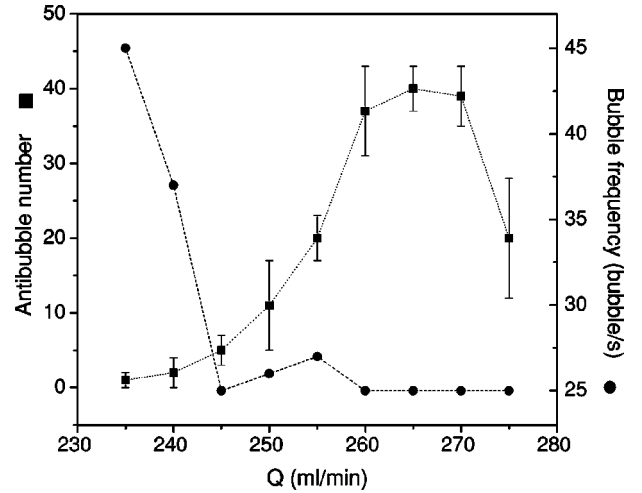


FIG. 13. Average number of antibubbles (squares) that can be observed simultaneously, and bubbling mean frequency (circles) as a function of the air flow rate for the solution 34/66 (2.6 cP). The dashed lines are guides to the eye.

chain of rising bubbles inside the liquid flow, like the patterns shown in Figs. 4 and 7. This liquid flows upward very fast around the bubble chain at the center of the liquid column up to the interface, forming a toroidal eddy at the top of the liquid column around the bubble chain. Closing the circuit, the liquid flows downward near the container wall toward the nozzle. Immersed in this flow, the antibubble is launched violently with the bubbles, and when it reaches the top of the liquid column, the antibubble changes its direction abruptly, crossing over toward the wall, and starts moving downward toward the nozzle slowly, following the liquid flow. The antibubbles persist for time intervals ranging from seconds up to 1 h, with an average time around 1 min, breaking into ordinary tiny bubbles. The balance between creation and annihilation gives the antibubble number. With this setup we have obtained antibubbles more persistent than those in a static bath [1] reported in the literature.

V. CONCLUSION

Here we focused on the evolution to the regime of formation of antibubbles due to the coalescence between two bubbles, created at a nozzle submerged in a viscous fluid. The mechanism of antibubble formation is related to droplets, which occur in the bubbling in a period-4 attractor, whenever a spike of liquid penetrates upward inside a large bubble, generated by the coalescence, until the interface is broken up and a small fluid drop is formed inside the bubble. When some of these droplets encounter the inner bubble surface, a layer of air is trapped around the droplets. The antibubbling regime is a complex system in which a heterogeneous amalgam of different phenomena occurs, like bubbling followed by period doubling, discontinuity in the dynamics characterized by coalescence, inverted dripping as a result of the instability of the Rayleigh jet, and finally the appearance of antibubbles as the outcome of the intermittency and liquid circulation. The transition to chaos via intermittency influ-

ences the creation, while ordered liquid flow stabilizes the antibubble, allowing the spherical shell of air to have uniform thickness, creating antibubbles more persistent than those of a static bath.

ACKNOWLEDGMENTS

This work was partially supported by the Brazilian Agencies CNPq and FAPESP.

-
- [1] C. L. Stong, *Sci. Am.* **4**, 116 (1974). For an introduction to antibubbles we recommend this webpage: <http://www.jtan.com/antibubble/>
- [2] A. Tufaile and J. C. Sartorelli, *Phys. Lett. A* **287**, 74 (2001).
- [3] A. Tufaile and J. C. Sartorelli, *Physica A* **275**, 336 (2000).
- [4] A. Tufaile, R. D. Pinto, W. M. Gonçalves, and J. C. Sartorelli, *Phys. Lett. A* **255**, 58 (1999).
- [5] H. L. Anderson, *A Physicist's Desk Reference: The Second Edition of the Physics Vade Mecum* (Springer-Verlag, New York, 1989).
- [6] J. F. Davidson and B. O. G. Schüler, *Trans. Inst. Chem. Eng.* **38**, 144 (1960).
- [7] R. Clift, J. R. Grace, and M. E. Weber, *Bubbles, Drops, and Particles* (Academic Press, New York, 1978).
- [8] S. Chandrasekhar, *Hydrodynamic and Hydromagnetic Stability* (Dover, New York, 1981).
- [9] K. Nguyen, C. S. Daw, M. Cheng, D. D. Bruns, C. E. A. Finney, and M. B. Kennel, *Chem. Eng. J.* **64**, 191 (1996).
- [10] B. W. Zeff, B. Kleber, J. Fineberg, and D. P. Lathrop, *Nature (London)* **403**, 401 (2000).
- [11] R. Manasseh and N. Tracey, *Album of Visualization* **13**, 25 (1996).
- [12] M. S. Longuet-Higgins, *J. Fluid Mech.* **127**, 103 (1983).
- [13] M. C. Ruzicka, J. Drahos, J. Zahrádník, and N. H. Thomas, *Int. J. Multiphase Flow* **23**, 671 (1997).
- [14] D. J. Tritton and C. Egdell, *Phys. Fluids A* **5**, 503 (1993).